

The influence of microchannel internal structure elements spatial distribution on the hydrodynamic characteristics of the fluid flow

© N.B. Fatkullina, S.S. Kurbanova, O.A. Solnyshkina

Ufa University of Science and Technology, Ufa, Russia
E-mail: sabina_kurbanova_2004@mail.ru

Received May 3, 2024

Revised July 11, 2024

Accepted October 30, 2024

This study applies a numerical approach to describe the flow behaviour in a microchannel with non-deformable structural elements. The influence of the spatial distribution of the channel internal structure elements on the integral characteristics of the system is studied. In particular, the change of permeability of the model at different values of the specific surface area of the channel elements and at transition to the second porosity scale with preservation of the total porosity of the system is considered. Flow patterns and velocity fields in channels of complex geometry are obtained. The dependence of the medium permeability on the spatial distribution of micro-sized posts inside the channel is also determined.

Keywords: Hydrodynamics, Stokes flows, double porosity, microchannels.

DOI: 10.61011/TPL.2024.12.60348.6505k

In recent years, an upsurge in production of three-dimensional chips, where several substrates with electronic components are positioned in parallel at a distance of 50–100 μm , has been observed in the electronics industry. The three-dimensional structure of devices complicates the process of heat dissipation. This has led to an increased research interest in development of fluid microscale cooling systems [1]. In-depth knowledge of the hydrodynamic processes in microchannels is needed to design such systems. An approach to co-engineering of microfluidic systems and electronics and the results of efficiency measurements for a microchannel heat exchanger integrated into a 3D chip were presented in [2]. Compared to conventional heat exchangers, microscale ones have certain specific operational features that require a more detailed examination. One important factor that must be taken into account in the process of design of microscale heat exchangers is the geometry of the structure, since it should provide the largest possible heat exchange surface area at an acceptable level of hydrodynamic losses.

The influence of channel cross section variations and added finning on the heat transfer rate has been discussed in considerable detail in literature [3,4]. Microchannels with a complex internal structure (e.g., planar microchannels with distributed arrays of posts) are also used often at the present day to increase the efficiency of heat exchangers. The main features of the mentioned configuration are a larger area of contact between the surface and the coolant and better mixing in the flow. In most studies we reviewed, the shape of elements was varied [5] and simple cases of spatial arrangement of posts (in rows or in a checkerboard pattern [6] with equal distances between posts) were investigated. The issue of efficiency of two scales of packing for these elements remains open.

In this context, the aim of the present study is to investigate numerically the influence of the spatial distribution of posts inside a planar microchannel on hydrodynamic flows of a viscous fluid and the integral flow characteristics.

The periodic flow of a viscous fluid at a constant pressure difference in a rectangular microchannel with a complex internal structure (non-deformable cylindrical elements distributed across the flow) is considered. It is assumed that inertial forces are negligible, since the fluid flow is slow, which is typical of microscale processes. Thus, the steady fluid flow may be characterized by the Stokes equation and the continuity equation

$$-\nabla p + \mu \left(\frac{\partial^2 u_x}{\partial x^2} + \frac{\partial^2 u_y}{\partial y^2} + \frac{\partial^2 u_z}{\partial z^2} \right) = 0,$$

$$\frac{\partial u_x}{\partial x} + \frac{\partial u_y}{\partial y} + \frac{\partial u_z}{\partial z} = 0, \quad (1)$$

where p is the pressure; u_x , u_y , and u_z are the velocity vector components; and μ is the dynamic viscosity. The no-slip condition is set on specific channel area S_s (the total area of channel walls and non-deformable posts). The periodicity condition is set at the microchannel inlet and outlet

$$\mathbf{u}|_{x=0} = \mathbf{u}|_{x=L} = \mathbf{u}_S, \quad \mathbf{f} = \boldsymbol{\sigma} \cdot \mathbf{n},$$

$$\mathbf{f}|_{x=L} = -\mathbf{f}|_{x=0} + \mathbf{f}_p = -\mathbf{f}_S + \mathbf{f}_p, \quad \mathbf{f}_p = \mathbf{i}_x \Delta p, \quad (2)$$

where \mathbf{n} is the surface normal; \mathbf{x} is the radius vector of the point under consideration; \mathbf{f} is the difference of normal stress vectors; $\boldsymbol{\sigma}$ is the stress tensor; L is the length of a fragment of the computational domain or the periodicity scale in direction x ; S is the channel inlet section subscript; and p denotes the addition to the stress vector corresponding to a given pressure difference.

Numerical experiments were performed using the pre-developed 3D boundary element method accelerated by

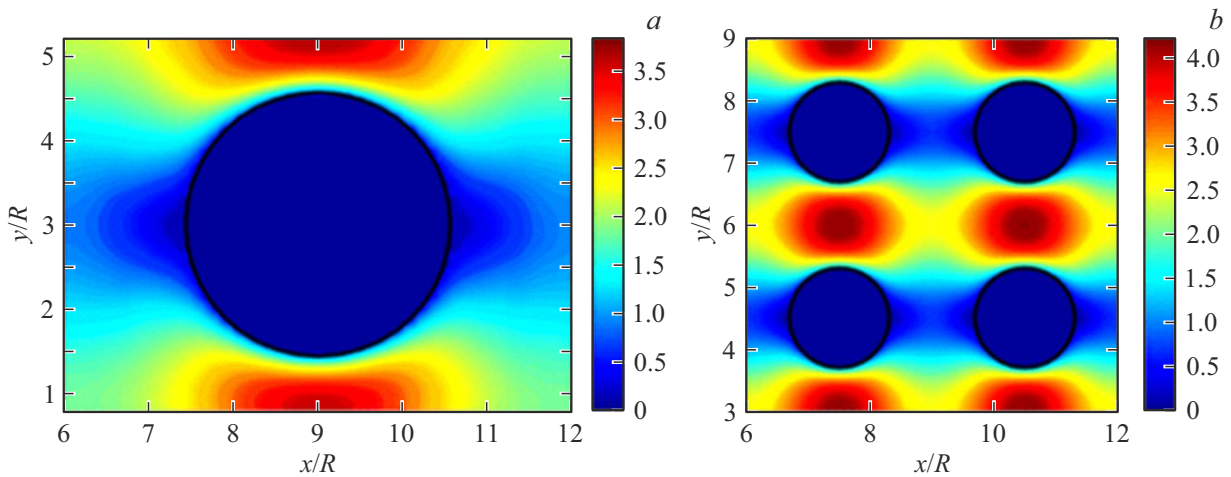


Figure 1. Fields of the averaged velocity modulus in the channel at $k_s = 1$ (a) and 0.25 (b).

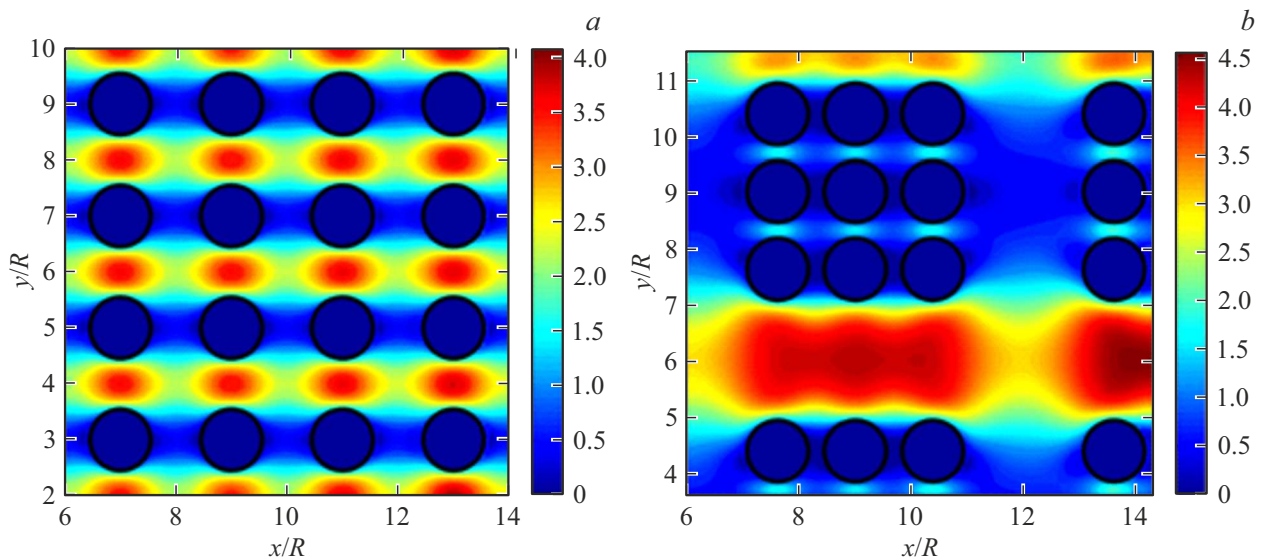


Figure 2. Fields of the averaged velocity modulus in the channel at $k_r = 1$ (a) and 2.5 (b).

the fast multipole method on heterogeneous computing architectures [7,8]. This method provides an opportunity to apply a grid just to the surfaces of examined elements instead of covering the entire computational domain, thus reducing significantly the computational complexity for three-dimensional problems. We have already compared the results obtained using the developed software modules with experimental data on fluid flow in microchannels with dual porosity [7]. A fine agreement between experimental and computational data was demonstrated.

Numerical experiments on the flow of a viscous incompressible fluid in planar microchannels with different distributions of posts (the channel length, width, and height were $180\ \mu\text{m}$, $120\ \mu\text{m}$, and $10\ \mu\text{m}$, respectively) were carried out in the present study. Their number and spatial distribution were varied at the same porosity scale. To establish a second porosity scale with the same number of

posts, their arrangement was altered by isolating groups of nine posts and varying the distance both between groups and between posts within a group. The total porosity remained constant at $m = 0.8$, since it is defined as the ratio of the void volume to the volume of the entire channel together with the elements. In the first design, the number of structural elements varied from 1 to 4. A coefficient equal to the ratio of the cross-sectional area of a single post to the total cross-sectional area of all elements (k_s) was introduced for convenience. In the second case, the widths of wide (w_b) and narrow (w_s) pore channels were used to estimate the hydraulic radius of the formed channels:

$$r_b = hw_b/2(h + w_b), \quad r_s = hw_s/2(h + w_s),$$

where h is the channel height. Ratio k_r of the hydraulic radius of a wide channel to the hydraulic radius of a narrow channel is a geometric coefficient that affects the

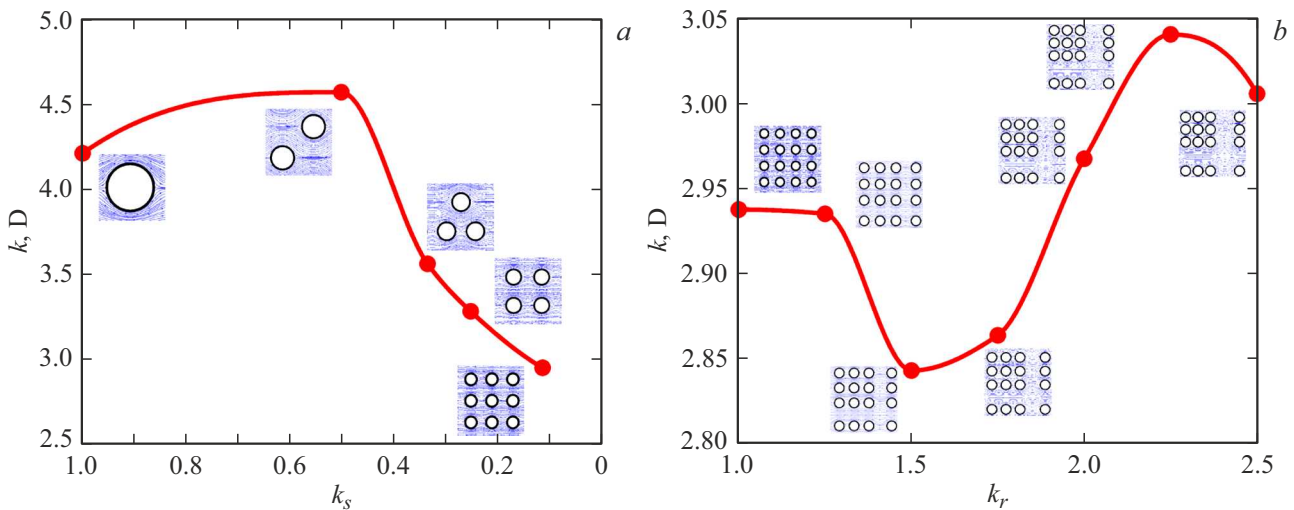


Figure 3. *a* — Dependence of permeability on coefficient k_s in the model with one porosity scale. Blocks in the figure are associated with coefficient k_s : the smaller it is, the greater is the number of elements in a block. *b* — Dependence of permeability on ratio k_r of hydraulic radii in the dual porosity model. Blocks in the figure are associated with k_r : as this parameter increases, the distance between arrays in the channel also increases, while the distance between array elements decreases.

flow pattern in the channel as a whole. The ratio of hydraulic radii of wide and narrow pore channels in the examined designs varied from 1 to 2.5. Flow patterns for a viscous incompressible fluid in channels at $k_s = 0.25–1$ were obtained. Figure 1 shows the fields of averaged absolute flow velocity in channels with coefficient $k_s = 1$ and 0.25. Diameters d of cylindrical elements in the channels were 30.27 and $15.13 \mu\text{m}$, respectively.

It was demonstrated that the maximum fluid flow velocity increases with an increase in coefficient k_s and, consequently, with an increase in the specific surface area of elements at constant porosity. The main fluid flow is concentrated in longitudinal regions between the elements, and the maximum velocity is observed in the middle of the gap between posts. Such calculations of the velocity field were carried out for channels with two porosity scales (Fig. 2). Flow patterns for channels with hydraulic radii ratios $k_r = 1$ and 2.5 were obtained. A flow redistribution is observed in transition to the second porosity scale. Regions with significantly higher flow velocities emerge in longitudinal channels between arrays of posts.

The permeability of designed structures, which determines the throughput capacity, is crucial for their efficient application in microscale heat exchangers. The higher the permeability of the medium is, the greater volume of fluid may be passed through it with minimal power consumption and the higher is the efficiency of microchip cooling. It is known that the specific surface area through which the flow passes affects directly the absolute permeability of the medium. The larger the specific surface area is, the greater is the area of contact between phases, and this may contribute to an increase in permeability of the medium. However, in certain cases, an increase in specific surface area may result in a reduction in permeability due

to capillary effects. In addition, the integral characteristics of the medium are affected to a significant degree by the spatial distribution of its specific surface area. The absolute permeability of all models was estimated. Figure 3 presents the dependences of absolute permeability of the channel on coefficient k_s for the model with one porosity scale (*a*) and on ratio k_r of hydraulic radii in the case of dual porosity (*b*).

In the case of one porosity scale, the channel permeability tends to decrease with an increase in specific surface area (i.e., with a reduction in coefficient k_s). However, $k_s = 0.5$ falls out of this pattern, which is attributable to an increase in hydraulic resistance with this arrangement of structures. Insets with images of channels corresponding to different coefficient k_s values are shown in Fig. 3, *a* for clarity. The pattern changes in the dual porosity model. At $k_r = 1.25$, this model has the properties of a medium with one porosity scale, and the absolute permeability remains practically unchanged. As the ratio of hydraulic radii increases, the distance between the arrays of posts also increases, while the elements themselves become closer to each other. The throughput capacity of narrow channels between the posts is minimized, and the main fluid flow passes through wide channels between the arrays. At $k_r = 2.5$, the free space in element arrays becomes critically small, inducing a flow redistribution and a reduction in permeability of the system. This has a significant influence on the absolute permeability of the channel. The permeability tends to increase with increasing k_r , which is illustrated in Fig. 3, *b*, where insets with images of channels with increasing ratios of hydraulic radii are shown.

Thus, it was demonstrated that the specific surface area of the medium has a significant effect on its permeability, and the nature of this influence may vary depending on

the specific medium type and the operation conditions. With the channel permeability and the average fluid flow velocity taken into account, the optimum configuration is a channel with one porosity scale at $k_s = 0.5$ (two diagonally positioned cylinders with cross-sectional diameter $d = 21.4 \mu\text{m}$). This microchannel structure may be used efficiently in the design of, e.g., microscale heat exchangers, since it provides a high velocity of cross flows and fine permeability of the system, allowing one to achieve optimum device performance, minimize hydrodynamic losses, and enhance the efficiency of heat removal.

Funding

This study was supported by the Russian Science Foundation, grant № 24-19-00697 (<https://rscf.ru/project/24-19-00697/>).

Conflict of interest

The authors declare that they have no conflict of interest.

References

- [1] W. He, J. Zhang, R. Guo, C. Pei, H. Li, S. Liu, J. Wei, Y. Wang, *Appl. Energy*, **327**, 120048 (2022). DOI: 10.1016/j.apenergy.2022.120048
- [2] R. van Erp, R. Soleimanzadeh, L. Nela, G. Kampitsis, E. Matioli, *Nature*, **585**, 211 (2020). DOI: 10.1038/s41586-020-2666-1
- [3] M.Q. Ansari, G. Zhou, *Chem. Eng. Process.: Process Intensif.*, **156**, 108066 (2020). DOI: 10.1016/j.ccep.2020.108066
- [4] K. Derakhshanpour, R. Kamali, M. Eslami, *Int. Commun. Heat Mass Transfer*, **119**, 104928 (2020). DOI: 10.1016/j.icheatmasstransfer.2020.104928
- [5] N. Zhang, B. Jiao, Y. Ye, Y. Kong, X. Du, R. Liu, B. Cong, L. Yu, S. Jia, K. Jia, *Energy Convers. Manag.*, **253**, 115124 (2022). DOI: 10.1016/j.enconman.2021.115124
- [6] W. Yubing, J. Li, D. Zhang, W. Chen, G. Zhu, *Heat Mass Transfer*, **59**, 1543 (2023). DOI: 10.1007/s00231-023-03353-z
- [7] O.A. Solnyshkina, E.S. Batyrshin, Yu.A. Pityuk, *Fluid Dyn.*, **56** (4), 451 (2021). DOI: 10.1134/S001546282104011X
- [8] Y.A. Pityuk, O.A. Abramova, N.B. Fatkullina, A.Z. Bulatova, in *Recent research in control engineering and decision making*, ed. by O. Dolinina, A. Brovko, V. Pechenkin, A. Lvov, V. Zhmud, V. Kreinovich, *Studies in Systems, Decision and Control* (Springer, Cham, 2019), vol. 199, p. 338–352. DOI: 10.1007/978-3-030-12072-6_28

Translated by D.Safin